J. Phys. B: At. Mol. Opt. Phys. **33** (2000) 4053–4067. Printed in the UK PII: S0953-4075(00)50649-X

Atomic Bose–Einstein condensation with three-body interactions and collective excitations

A Gammal†, T Frederico‡, Lauro Tomio† and Ph Chomaz§

† Instituto de Física Teórica, Universidade Estadual Paulista, 01405-900 São Paulo, Brazil
‡ Departamento de Física, Instituto Tecnológico da Aeronáutica, Centro Técnico Aeroespacial, 12228-900 São José dos Campos, SP, Brazil
§ GANIL, BP 5027, F-14021 Caen Cedex, France

Received 28 April 2000

Abstract.

The stability of a Bose–Einstein condensed state of trapped ultra-cold atoms is investigated under the assumption of an attractive two-body and a repulsive three-body interaction. The Ginzburg–Pitaevskii–Gross (GPG) nonlinear Schrödinger equation is extended to include an effective potential dependent on the square of the density and solved numerically for the s-wave. The lowest collective mode excitations are determined and their dependences on the number of atoms and on the strength of the three-body force are studied. The addition of three-body dynamics can allow the number of condensed atoms to increase considerably, even when the strength of the three-body force is very small compared with the strength of the two-body force. We study in detail the first-order liquid–gas phase transition for the condensed state, which can happen in a critical range of the effective three-body force parameter.

1. Introduction

The theoretical research on Bose–Einstein condensation (BEC) [1], a phenomenon predicted more than 70 years ago, has received considerable experimental and theoretical support in recent years [2]. The relevance of BEC for understanding the properties of liquid ^{4}He was pointed out by London [3], suggesting that the peculiar phase transition that liquid helium undergoes at 2.18 K is a BEC phenomenon. It is also important to observe that, at the level of two-body collisions, Bogoliubov in 1947 [4] has shown for a homogeneous gas that BEC is only possible for systems with repulsive potentials.

Intense experimental research on BEC for magnetically trapped weakly interacting atoms have been done recently [5–8]. In the experiment reported in [5], a condensate of approximately 2000 spin-polarized ^{87}Rb atoms was produced in a cylindrically symmetric magnetic trap [2, 9]. It is a common understanding that, at low temperature and density, where interatomic distances are much greater than the distance scale of atom–atom interactions, two-body interactions take a simple form and three-body interactions can be neglected. In such a regime, only two-body s-wave scattering is important. With a low enough temperature the magnitude of the scattering length a is much less than the corresponding thermal de Broglie wavelength, and the exact shape of the two-atom interaction is unimportant.

The experimental evidence of Bose–Einstein condensation in magnetically trapped weakly interacting atoms [5–8] has brought considerable support to the theoretical research on bosonic condensation. The nature of the effective atom–atom interaction determines the stability of

0953-4075/00/194053+15$30.00 © 2000 IOP Publishing Ltd

the condensed state: the two-body pseudopotential is repulsive for a positive s-wave atom–atom scattering length and it is attractive for a negative scattering length [10]. The ultra-cold trapped atoms with repulsive two-body interaction undergo a phase transition to a stable Bose condensed state, in several cases found experimentally, such as for ^{87}Rb [5], ^{23}Na [7] and ^{1}H [8]. However, a condensed state of atoms with a negative s-wave atom–atom scattering length (as in the case of ^{7}Li [6]) would be unstable, unless the number of atoms N is small enough such that the stabilizing force provided by the harmonic confinement in the trap overcomes the attractive interaction, as found on theoretical grounds [11, 12]. It was indeed observed in the ^{7}Li gas [6], for which the s-wave scattering length is $a = -14.5 \pm 0.4$ Å, that the number of allowed atoms in the Bose condensed state was limited to a maximum value of between 650 and 1300, which is consistent with the mean-field prediction [11].

So, for systems of atoms with attractive two-body interaction, it is widely believed [11, 13, 14] that the condensate has no stable solution above a certain critical number of atoms $N_{\max}$. However, as reported in [15, 16], the addition of a repulsive potential derived from three-body interactions is consistent with a number of atoms larger than $N_{\max}$. Even for a very small strength of the three-body force, the region of stability for the condensate can be extended considerably. By considering the possible effective interactions, it was reported in [17] that a sufficiently dilute and cold Bose gas exhibits similar three-body dynamics for both signs of the s-wave atom–atom scattering length. It was also suggested that, for a large number of bosons the three-body repulsion can overcome the two-body attraction, and a stable condensate will appear in the trap [18]. If an atomic system is characterized by having effectively an attractive two-body interaction together with a repulsive three-body interaction, two mechanisms for stability are possible: (a) the kinetic energy acting at lower densities and (b) the repulsive weak three-body force effective at higher densities. These mechanisms indicate that, for the same number of atoms, one lower-density phase and a higher-density phase can be found, if the three-body force is weak enough not to dominate the effective interaction.

It was pointed out in [19] that an easier experimental approach to probing density fluctuations is to consider an observable directly sensitive to the probability of finding three atoms near each other, which will correspond to the loss rate of atoms due to three-body recombination. Such a three-body recombination rate in BEC was considered recently in [14, 20, 21] (see also the review of [13]). It was shown in [20] that the three-body recombination coefficient of ultracold atoms to a weakly bound s level goes to infinity in the Efimov limit [22]. The Efimov limit is a particularly interesting three-body effect, which happens when the two-body scattering length is very large (positive or negative). In this case, with the two-boson energy close to zero, the three-boson system presents an increasing number of loosely bound three-body states, which have large spatial extension and do not depend on the details of the interaction [23].

So, our main motivation is to provide an extension to the Ginzburg–Pitaevskii–Gross (GPG) equation [24, 25], which considers a three-body interaction and, in this way, provides the framework for a numerical investigation of the relevance of the three-body interaction in Bose–Einstein condensation. Recently, we presented a first dynamical approach in this direction [26], where it was shown that the decay time of a trapped atomic system (as considered in the present paper) that starts in a denser (liquid) phase is longer than expected due to strong oscillations of the mean-squared radius. As observed in [26], such oscillations of the mean-squared radius also happen if the real part of the three-body effective potential, parametrized by λ_3 (or g_3 in dimensionless units), is zero. The collapse 'burns' the atoms in the states with higher densities and explains a sudden increase of the square radius after each compression, with the atoms remaining in dilute states. The inclusion of the repulsive three-body force still

maintains the oscillatory mode, but the compression is not as dramatic as in the former case and, consequently, atoms in higher-density states are not so efficiently burned. In the situation when the three-body repulsion dominates over the two-body attraction, the condensate can be in a denser phase where it is expected to be strongly unstable due to recombination losses. However, the dynamics of the condensate is modulated by an oscillatory mode with a frequency nearly twice that of the trap†, as also found when $\lambda_3 = 0$ [28]. In the case of $\lambda_3 > 0$, the oscillatory mode dominates the dynamics of the condensate, implying density fluctuation and thus the condensate does not decay as quickly as expected.

In this paper we consider a possible general scenario of atomic systems with attractive two-body and repulsive three-body interactions, extending previous studies considered in [16, 26]. The lowest collective mode excitations are also determined and their dependences on the number of atoms and on the strength of the three-body force are studied. We show that, in a dilute gas, a small repulsive three-body force added to an attractive two-body interaction is able to stabilize the condensate beyond the critical number of atoms in the trap, found just with an attractive two-body force [11], such that a kind of liquid–gas phase transition occurs. By using the mean-field approximation, we investigate the competition between the leading term of an attractive two-body interaction, originated from a negative two-atom s-wave scattering length, and a repulsive three-body effective interaction, which can happen near the Efimov limit [22] ($|a| \to \infty$) as discussed in [17]‡. With respect to the realization of the above scenario, we note that recently the possibility of continuously altering the two-body scattering length, from positive to negative values, by means of an external magnetic field was reported [30]. This was further investigated in optically trapped caesium gas [31]. By tuning the two-body scattering length, one can approach the Efimov limit, where new physics is expected. The first step to understanding the new physics that can happen as one approaches this limit is to consider the situation in which the three-body effect is not negligible.

The paper is organized as follows. In section 2, we introduce the Ginzburg–Pitaevskii–Gross formalism. In section 3, we present the main numerical results for the static solutions, together with a variational analysis. In section 4, we present a stability analysis and results for collective excitation in the condensate. In this section 4 we also observe that the inclusion of three-body effects points out possible evidence of a liquid–gas phase transition in the condensate. Finally, in section 5, we present our main conclusions.

2. Ginzburg–Pitaevskii–Gross formalism

In the following, we present our formalism, where the original Ginzburg–Pitaevskii–Gross nonlinear equation [24, 25], which includes a term proportional to the density (two-body interaction), is extended through the addition of a term proportional to the density squared (a three-body interaction). Next, after reducing such an equation to dimensionless units, we study numerically the s-wave solution by varying the corresponding dimensionless parameters, which are related to the two-body scattering length, the strength of the three-body interaction and the number of atoms in the condensed state. As particularly observed in [32], to incorporate all two-body scattering processes in such a many-particle system, the two-body potential should be replaced by the many-body T-matrix. Usually, at very low energies, this is approximated by the two-body scattering matrix, which is directly proportional to the scattering length [12]. So, in order to obtain the desired equation, we first consider the effective Lagrangian, which

† Also clarified in [27] by using the virial approach.
‡ See [23, 29] for the universal aspects of the Efimov limit.

describes the condensed wavefunction in the Hartree approximation, implying the GPG energy functional

$$\mathcal{L} = \int \mathrm{d}^3 r \left[\frac{\mathrm{i}\hbar}{2} \Psi^\dagger(\vec{r}) \frac{\partial \Psi(\vec{r})}{\partial t} - \frac{\mathrm{i}\hbar}{2} \frac{\partial \Psi^\dagger(\vec{r})}{\partial t} \Psi(\vec{r}) + \frac{\hbar^2}{2m} \Psi^\dagger(\vec{r}) \nabla^2 \Psi(\vec{r}) - \frac{m}{2} \omega^2 r^2 |\Psi(\vec{r})|^2 \right] + \mathcal{L}_{\mathrm{I}}. \tag{1}$$

In our description, the atomic trap is given by a rotationally symmetric harmonic potential, with angular frequency ω, and $\mathcal{L}_{\mathrm{I}}$ gives the effective atom interactions up to three particles. The effective interaction Lagrangian for ultra-low temperature bosonic atoms, including two- and three-body scattering at zero energy, is written as

$$\begin{aligned} \mathcal{L}_{\mathrm{I}} = -\tfrac{1}{2} \int \mathrm{d}^3 r_1 \, \mathrm{d}^3 r_2 \, \mathrm{d}^3 r_1' \, \mathrm{d}^3 r_2' \, \Psi^\dagger(\vec{r_1'}) \Psi^\dagger(\vec{r_2'}) \Psi(\vec{r}_1) \Psi(\vec{r}_2) \langle \vec{r_{12}'} \left| T^{(2)}(0) \right| \vec{r}_{12} \rangle \\ \times \delta^3(\vec{r}_1' + \vec{r}_2' - \vec{r}_1 - \vec{r}_2) - \frac{1}{3!} \int \prod_{i=1}^{3} \left(\mathrm{d}^3 r_i \, \mathrm{d}^3 r_i' \, \Psi^\dagger(\vec{r}_i') \Psi(\vec{r}_i) \right) \delta^3(\vec{R}_{123}' - \vec{R}_{123}) \\ \times \left\langle \vec{r}_{12}' \vec{R}_3' \left| T^{(3)}(0) - \sum_{j<k} T_{jk}^{(2)}(0 - K_i) \right| \vec{r}_{12} \vec{R}_3 \right\rangle \end{aligned} \tag{2}$$

where $\vec{r}_{12}$ and $\vec{R}_3$ are the relative coordinates, given by $\vec{r}_{12} = \vec{r}_1 - \vec{r}_2$ and $\vec{R}_3 = \vec{r}_3 - (\vec{r}_1 + \vec{r}_2)/2$; and $\vec{R}_{123} \equiv (\vec{r}_1 + \vec{r}_2 + \vec{r}_3)$. $T^{(3)}(0)$ and $T_{jk}^{(2)}(0)$ are the corresponding three- and two-body T-matrices, which are evaluated at zero energy. The two-body T-matrix for each pair (jk) is subtracted from $T^{(3)}(0)$ to avoid double counting and K_i is the kinetic energy operator for particle i.

We can approximate the above effective interaction Lagrangian at low densities by averaging the T-matrices over the relative coordinates, considering that the thermal wavelength is much greater than the characteristic interaction distances,

$$\begin{aligned} \mathcal{L}_{\mathrm{I}} = -\tfrac{1}{2} \int \mathrm{d}^3 r_{12}' \, \mathrm{d}^3 r_{12} \, \langle \vec{r_{12}'} | T^{(2)}(0) | \vec{r}_{12} \rangle \int \mathrm{d}^3 r \, |\Psi(\vec{r})|^4 - \frac{1}{3!} \int \mathrm{d}^3 r_{12}' \, \mathrm{d}^3 R_3' \, \mathrm{d}^3 r_{12} \, \mathrm{d}^3 R_3 \\ \times \int \mathrm{d}^3 r \, |\Psi(\vec{r})|^6 \left\langle \vec{r_{12}'} \vec{R}_3' \left| T^{(3)}(0) - \sum_{j<k} T_{jk}^{(2)}(0 - K_i) \right| \vec{r}_{12} \vec{R}_3 \right\rangle. \end{aligned} \tag{3}$$

The integrations of the T-matrices over the relative coordinates give the zero-momentum matrix elements:

$$\int \mathrm{d}^3 r_{12}' \, \mathrm{d}^3 r_{12} \, \langle \vec{r_{12}'} \left| T^{(2)}(0) \right| \vec{r}_{12} \rangle = (2\pi)^3 \langle \vec{p}_{12} = 0 \left| T^{(2)}(0) \right| \vec{p}_{12} = 0 \rangle = \frac{4\pi\hbar^2 a}{m} \tag{4}$$

where a is the two-body scattering length. For the connected three-body T-matrix, also by integrating over the coordinates, we obtain the corresponding zero-momentum ($\vec{p}_{12} = 0$, $\vec{P}_3 = 0$) matrix elements, which give us the strength of the three-body effective interaction λ_3, as follows:

$$\begin{aligned} \int \mathrm{d}^3 r_{12}' \, \mathrm{d}^3 R_3' \, \mathrm{d}^3 r_{12} \, \mathrm{d}^3 R_3 \left\langle \vec{r_{12}'} \vec{R}_3' \left| T^{(3)}(0) - \sum_{j<k} T_{jk}^{(2)}(0 - K_i) \right| \vec{r}_{12} \vec{R}_3 \right\rangle \\ = (2\pi)^6 \left\langle \left| T^{(3)}(0) - \sum_{j<k} T_{jk}^{(2)}(0 - K_i) \right| \right\rangle = 2\lambda_3 \end{aligned} \tag{5}$$

where $\langle \, | \equiv \langle \vec{p}_{12} = 0, \vec{P}_3 = 0 |$ and $| \, \rangle \equiv | \vec{p}_{12} = 0, \vec{P}_3 = 0 \rangle$.

The nonlinear Schrödinger equation, which describes the condensed wavefunction in the mean-field approximation, is obtained from the effective Lagrangian given in equation (1). By considering the interaction in equation (3), it can be written as [33]

$$\mathrm{i}\hbar\frac{\partial\Psi(\vec{r},t)}{\partial t}=\left[-\frac{\hbar^2}{2m}\nabla^2+\frac{m}{2}\omega^2r^2-N\frac{4\pi\hbar^2|a|}{m}|\Psi(\vec{r},t)|^2+\lambda_3N^2|\Psi(\vec{r},t)|^4\right]\Psi(\vec{r},t). \tag{6}$$

For a stationary solution, $\Psi(\vec{r},t)=\mathrm{e}^{-\mathrm{i}\mu t/\hbar}\ \psi(\vec{r})$, and the above equation can be written as

$$\mu\psi(\vec{r})=\left[-\frac{\hbar^2}{2m}\nabla^2+\frac{m}{2}\omega^2r^2-N\frac{4\pi\hbar^2|a|}{m}|\psi(\vec{r})|^2+\lambda_3N^2|\psi(\vec{r})|^4\right]\psi(\vec{r}) \tag{7}$$

where μ is the chemical potential (single-particle energy) and $\psi(\vec{r})$ is normalized as

$$\int\mathrm{d}^3r\,|\psi(\vec{r})|^2=1. \tag{8}$$

The total energy of the system is given by

$$E=\int\mathrm{d}^3r\left\{N\frac{\hbar^2}{2m}\,|\nabla\psi(\vec{r})|^2+N\frac{m}{2}\omega^2r^2\,|\psi(\vec{r})|^2-\frac{N^2}{2}\frac{4\pi\hbar^2|a|}{m}|\psi(\vec{r})|^4+\frac{N^3}{3}\lambda_3|\psi(\vec{r})|^6\right\}. \tag{9}$$

The central density of the system can be obtained directly from the solution of the above equation, normalized as in equation (8):

$$\rho_c=N|\psi(0)|^2. \tag{10}$$

The physical scales presented in the above equations can be easily recognized by working with dimensionless equations. By rescaling equation (7) for the s-wave solution, we obtain

$$\left[-\frac{\mathrm{d}^2}{\mathrm{d}x^2}+\frac{1}{4}x^2-\frac{|\Phi(x)|^2}{x^2}+g_3\frac{|\Phi(x)|^4}{x^4}\right]\Phi(x)=\beta\Phi(x) \tag{11}$$

where $x\equiv\sqrt{2m\omega/\hbar}r$ and $\Phi(x)\equiv N^{1/2}\sqrt{8\pi|a|}\ r\psi(\vec{r})$. The dimensionless parameters, related to the chemical potential and the three-body strength are, respectively, given by

$$\beta\equiv\frac{\mu}{\hbar\omega}\qquad\text{and}\qquad g_3\equiv\lambda_3\hbar\omega\left[\frac{m}{4\pi\hbar^2a}\right]^2. \tag{12}$$

The normalization for $\Phi(x)$, obtained from equation (8), defines a number n related to the number of atoms N:

$$\int_0^\infty\mathrm{d}x\,|\Phi(x)|^2=n\qquad\text{where}\quad n\equiv2N|a|\sqrt{\frac{2m\omega}{\hbar}}. \tag{13}$$

The boundary conditions in equation (11) are given by [11]

$$\begin{aligned}&\Phi(x\to0)\to0\\&\Phi(x\to\infty)\propto\exp\left(-\tfrac{1}{4}x^2+\left[\beta-\tfrac{1}{2}\right]\ln(x)\right).\end{aligned} \tag{14}$$

In terms of the dimensionless variables, the total energy of the system is given by

$$E=\hbar\omega N\int_0^\infty\mathrm{d}x\left\{\left|\frac{\mathrm{d}\phi(x)}{\mathrm{d}x}\right|^2+\frac{x^2\phi^2(x)}{4}-\frac{n\phi^4(x)}{2x^2}+\frac{n^2g_3\phi^6(x)}{3x^4}\right\} \tag{15}$$

where $\phi(x)\equiv\Phi(x)/n^{1/2}$ is normalized to one.

3. Liquid–gas phase transition: static solutions

3.1. Variational approach

As a further reference to our results, and the stability analysis, it will be helpful first to consider a variational procedure [34], using a trial Gaussian wavefunction for $\psi(\vec{r})$. So, in equation (9) we consider the following variational wavefunction (normalized to one):

$$\psi_{\rm var}(\vec{r}) = \left(\frac{1}{\pi\alpha^2}\frac{m\omega}{\hbar}\right)^{3/4} \exp\left[-\frac{r^2}{2\alpha^2}\left(\frac{m\omega}{\hbar}\right)\right] \tag{16}$$

where α is a dimensionless variational parameter. The corresponding root-mean-square radius, r_0, will be proportional to the variational parameter α:

$$r_0 \equiv \sqrt{\langle r^2\rangle_{\rm var}} = \alpha\sqrt{\frac{3\hbar}{2m\omega}}. \tag{17}$$

The expression for the total variational energy, which is obtained after replacing equation (16) in equation (9), is given by

$$E_{\rm var}(\alpha) = \hbar\omega N\left[\frac{3}{4}\left(\alpha^2 + \frac{1}{\alpha^2}\right) - \frac{n}{4\sqrt{\pi}\alpha^3} + \frac{2n^2 g_3}{9\sqrt{3}\pi\alpha^6}\right]. \tag{18}$$

In the same way, we can obtain the corresponding variational expression for the single-particle energy, equation (7):

$$\mu_{\rm var}(\alpha) = \hbar\omega\left[\frac{3}{4}\left(\alpha^2 + \frac{1}{\alpha^2}\right) - \frac{n}{2\sqrt{\pi}\alpha^3} + \frac{2n^2 g_3}{3\sqrt{3}\pi\alpha^6}\right]. \tag{19}$$

The variational central density, using equations (10) and (16), can also be given in terms of this parameter α:

$$\rho_{c,{\rm var}}(\alpha) = \left(\frac{m\omega}{\pi\hbar}\right)^{3/2}\frac{1}{\alpha^3}. \tag{20}$$

The approximate solutions for the total energy are obtained from the extrema of (18) with respect to variation of the parameter α. The variational solutions of $E_{\rm var}(\alpha)$ are given, as a function of n and g_3 (where $a < 0$ and $g_3 > 0$), by the real roots of $\partial E_{\rm var}(\alpha)/\partial\alpha = 0$†.

In figure 1, we first illustrate the variational procedure considering an arbitrarily small three-body interaction, chosen as $g_3 = 0.005$. In the upper part of the figure, we show five small plots for the total variational energy E, in terms of the variational width α. Each one of the small plots corresponds to particular values of n. For each number n we report the energy of the variational extrema in the lower part of figure 1. In region (I) where the number of atoms is still small, the attractive two-body force dominates over the repulsive three-body force and just one minima of the energy as a function of the variational parameter α is found. That is also the case for $g_3 = 0$. When the number of atoms is further increased (region (II)) two minima appear in the energy $E(\alpha)$. An unstable maximum is also found between the two minima. The lower-energy minimum is stable, while the solution corresponding to the smaller α is metastable. This solution has a higher density and, consequently, its metastability is justified by the repulsive three-body force acting at higher densities. The minimum number n for the appearance of the metastable state is characterized by an inflection point in the energy as a function of α. The value of n at the inflection point corresponds to the peak

† By using a numerical procedure one can easily reach the extrema of equation (18) by varying the parameter α, once the other parameters are fixed.

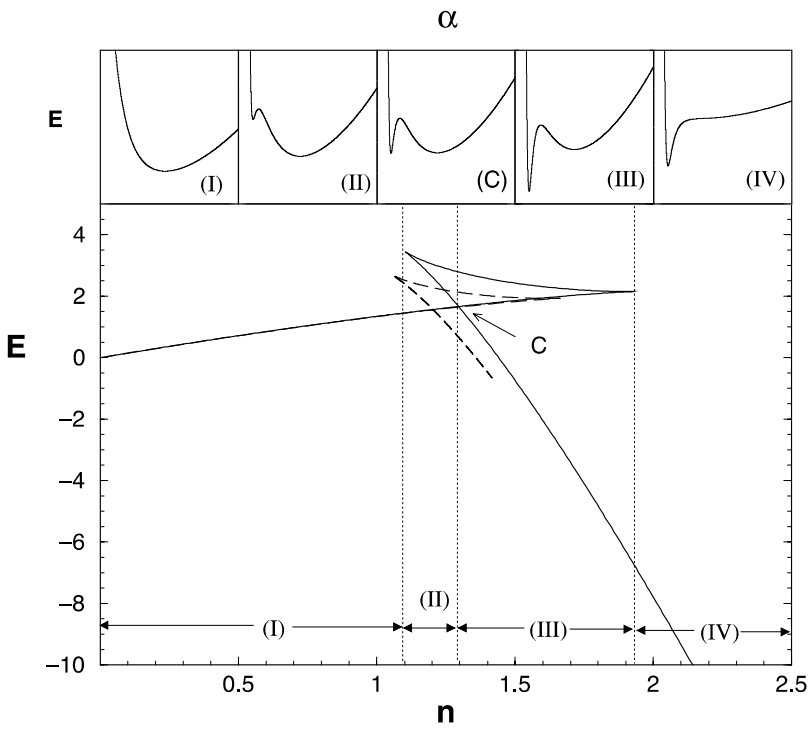

Figure 1. In the lower part, we have a comparison between variational (full curve) and exact (broken curve) numerical calculations of the condensate energy as a function of the reduced number of atoms n for $g_3 = 0.005$. In the upper frame we show five plots of the variational energy as a function of the variational parameter α for five particular values of n shown also in the lower frame. (I) (respectively IV) corresponds to a small (large) n region where only one stable solution is encountered; (II) (respectively III) to a small (large) n region where we observe three extrema for the energy; (C) corresponds to a particular n where we obtain two stable solutions with the same energy $E_1 = E_2$. E is given in units of $(N\hbar\omega)/n$.

in the plot of extremum energy versus n because for larger n three variational solutions are found as depicted in the lower part of figure 1. The attractive two-body and trap potentials dominate the condensed state in the low-density stable phase up to the crossing point (C). At this point, the denser metastable solution becomes degenerate in energy with the lower-density stable solution and a first-order phase transition takes place. Since the two solutions differ by their density this transition is analogous to a gas–liquid phase transition for which the density difference between the liquid and the gas is the order parameter. In the variational calculation this occurs at the transition number $n \approx 1.3$, while the numerical solution of the nonlinear Schrödinger equation (NLSE) gives 1.2. In region (III), we observe two local minima with different energies, a higher-density stable point and a lower-density metastable point. The metastable solution disappears in the peak at the boundary between region (III) and (IV). In regions (III) and (IV) the three-body repulsion stabilized a dense solution against the collapse induced by the two-body attraction. The qualitative features of the variational solution are clearly verified by the numerical solution of the NLSE, as shown by the broken curve.

3.2. Numerical results

The numerical solutions of equation (11) are obtained for several values of β, using three values of g_3 to characterize the solutions. We have used the Runge–Kutta (RK) and 'shooting' method to obtain the corresponding solutions in each case [35]. The stability assignment for the stationary solutions was made by studying the corresponding time-dependent Schrödinger equation, using the Crank–Nicolson (CN) method (see [11, 36]). The numerical procedure to determine such stability was done in the following way: when applying the CN method, we started by using the static solution obtained from the RK method and observed whether the modulus of the wavefunction remained constant. If this occurred for a long period of time (of about 500 units of dimensionless time $\tau = \omega t$) the solution was considered stable, otherwise it was considered unstable.

In figure 2 we present the total energy as a function of the number of atoms, represented by the reduced number n defined in equation (13), for three significative values of the quintic parameter g_3, given by 0, 0.016 and 0.03. The results agree with [15]. When $g_3 = 0$, the stable solutions for the energy start at zero (for $n = 0$) and reach a critical limit at $n_{\max} \simeq 1.62$. There are no solutions for higher n, but the plot also shows a branch with unstable solutions (with higher energies) for $n \leqslant 1.62$. Our results are consistent with results given in [32]. When $g_3 = 0.03$, only stable solutions appear for the energy, with no limit on the number of atoms, having a maximum at $n \sim 2$. So, this and higher values for g_3 already represent a dominance of the quintic term in the interaction of equation (11). We observe that the numerical stability analysis is consistent with the variational approach discussed in the previous subsection. The more interesting case represented in figure 2 is for $g_3 = 0.016$, as in such a case we observe

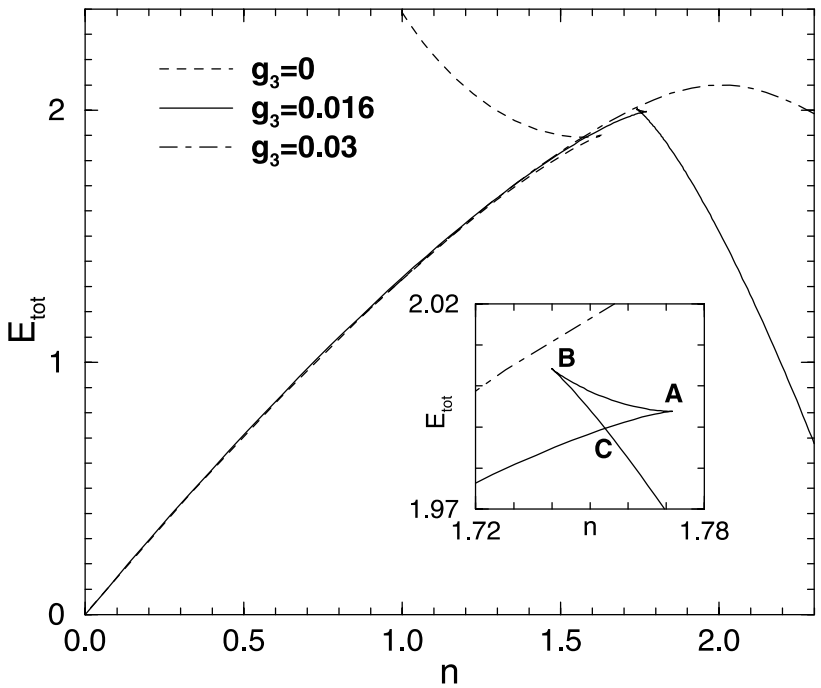

Figure 2. The total energy, in units of $(\hbar\omega)/\left(2|a|\sqrt{(2m\omega)/\hbar}\right)$, is shown as a function of the reduced number of atoms n, given by equation (13), for $g_3 = 0$, 0.016 and 0.03. The inset points out critical limits discussed in the text.

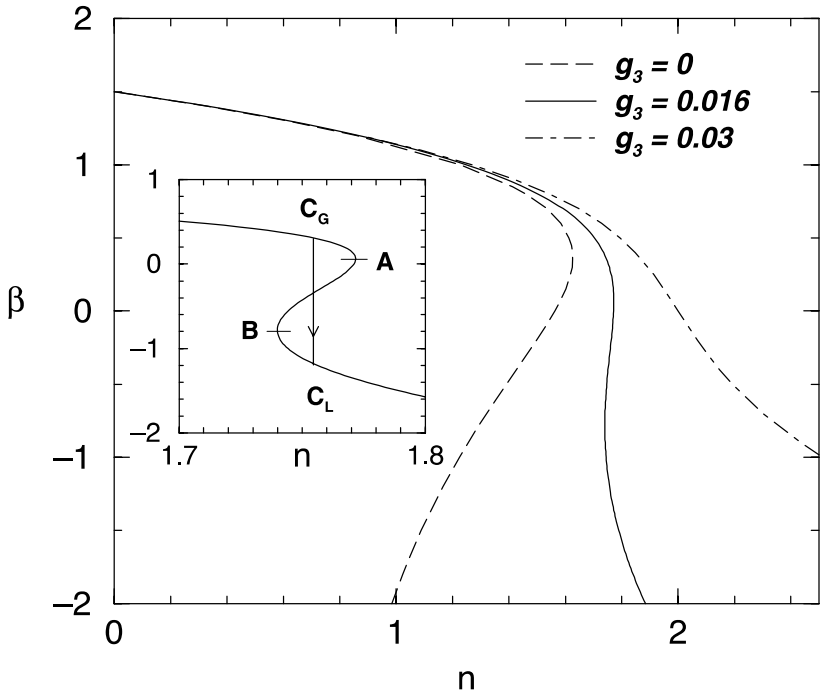

Figure 3. The chemical potential, in dimensionless units ($\beta = \mu/(\hbar\omega)$), is shown as a function of the reduced number of atoms n, for the same set of g_3 as shown in figure 2. The inset points out the critical limits corresponding to figure 2 (C_G and C_L correspond to C), and the straight line with an arrow indicates the transition from a less dense to a more dense phase.

a region of the plot where we can have up to three solutions for the same n. The inset to this figure amplifies the region of the plot where, for $g_3 = 0.016$, the solutions become unstable (between A and B) or metastable (between A and C, or B and C). At point C a phase transition occurs from a less dense (gas) to a more dense (liquid) phase.

In figure 3, following a correspondence to figure 2, we present the results for the chemical potential in dimensionless units (β) as a function of n. The line with an arrow in the inset to this figure indicates the approximate position in n where the phase transition (from a 'gas' phase to a 'liquid' phase) occurs. For $g_3 = 0.016$ the part of the plot linking points A and B is unstable (see both figures 2 and 3), otherwise it is stable. Finally, for $g_3 = 0.03$, the function of the energy in terms of n is always single valued and stable. Our calculation for $g_3 = 0$ also agrees with results presented in [11], with the maximum number of atoms limited to $n_{\max} \approx 1.62$†. As we can see, for $n \leqslant n_{\max}$ two solutions are possible, one of which is unstable. For g_3 higher than zero, a new pattern appears. For instance, the plot for the case of $g_3 = 0.016$ (see the inset) can be divided into several sectors according to the stability analysis, with the help of figure 2. Starting from $n = 0$ ($\beta = 1.5$) until point C_G, and from C_L to higher values of n, we have stable solutions; from C_G to A and from B to C_L we obtain metastable solutions; from A to B the solutions are unstable, corresponding to maxima for the energies.

In figure 4 we also plot the central density ρ_c, defined in equation (10), as a function of the number n. We use the same values of the parameter g_3 as used in figures 2 and 3. The inset to

† Our n is equal to $|C_{nl}^{3D}|$ of [11].

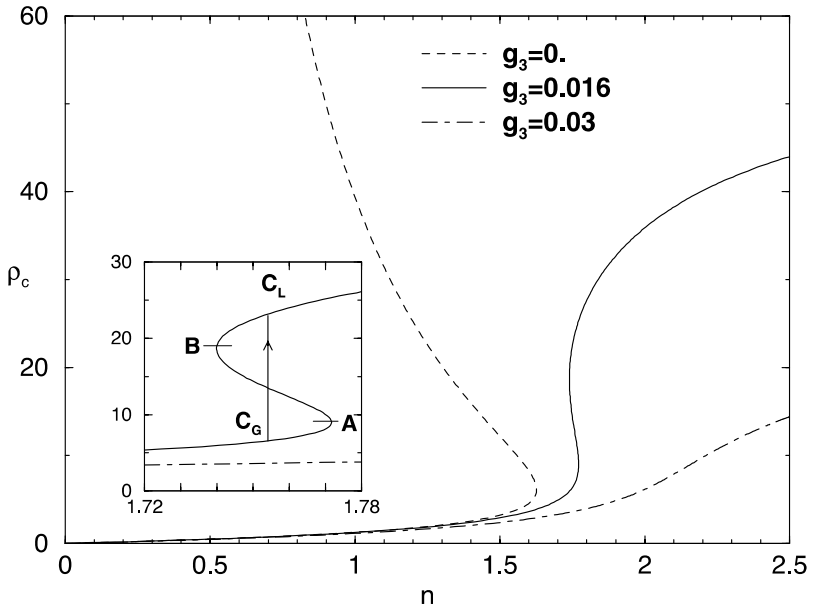

Figure 4. The central density, in dimensionless units, as a function of the number n, for the same set of parameters g_3 given in figures 2 and 3.

the figure also points out the phase transition which occurs when $g_3 = 0.016$. As the straight line with an arrow shows, after the transition the system becomes more than three times denser than the original one. Also, for $0 < g_3 < 0.0183$, we observe that the density ρ_c presents back bending typical of a first-order phase transition.

By extending the observations of a first-order phase transition, given in figures 2–4 for $g_3 = 0.016$, we also determined the region of g_3 where such kinds of phase transition can occur. In figure 5 we have a phase diagram, where the critical boundary separating the two phases and a critical point at $n = 1.8$ and $g_3 = 0.0183$ are shown. For g_3 less then such a critical value, we observe two regions with distinct phases, similar to gas and liquid phases. These two different phases are also clearly identified in our figure 4, where we present the central density as a function of n.

For each g_3, the transition point given by the crossing point in E versus n (see figure 2) corresponds to a Maxwell construction in the diagram of μ versus n. At this point an equilibrated condensate should undergo a phase transition from the branch extending to small n to the branch extending to large n. The system should never explore the back-bending part of the diagram because, as seen in figure 2, it is an unstable extremum of the energy. From figures 1–5, it is clear that the first branch is associated with small densities, large radii and positive chemical potentials, while the second branch presents a more compact configuration with a smaller radius, a larger density and a negative chemical potential. This justifies the term gas (G) for the first one and liquid (L) for the second one. However, we want to stress that both solutions are quantum fluids.

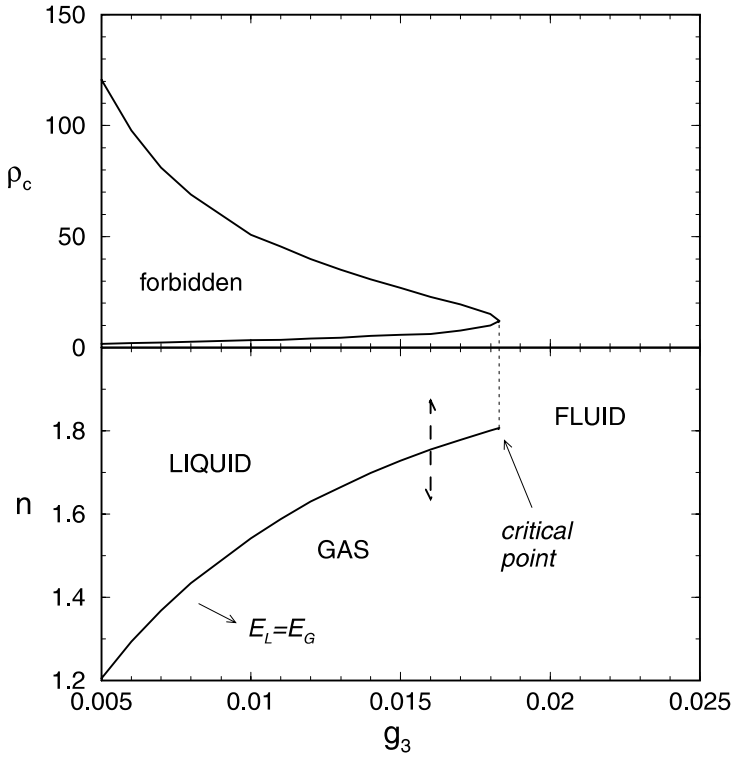

Figure 5. Graphical representation of the interface between the two distinct phases (gas and liquid), in the plane defined by the reduced number of atoms n and the parameter g_3 (lower frame); and for the central density ρ_c versus g_3 (upper frame). The arrows in the lower frame correspond to the point where the phase transition occurs for $g_3 = 0.016$, when changing n.

4. Collective excitations

In this section, from the time evolution of the GPG equation, given in equation (6), we consider the ground-state collective excitations for the system [37–39]. Following [39], the collective excitations are described by the Bogoliubov equations [4, 25, 34, 40]. After including three-body interactions they take the form

$$\begin{aligned}[\mathcal{L}_\nu - \hbar\omega_\nu]u_\nu + \left\{NU_0 + 2\lambda_3 N^2|\psi_g|^2\right\}[\psi_g]^2 v_\nu = 0 \\ [\mathcal{L}_\nu + \hbar\omega_\nu]v_\nu + \left\{NU_0 + 2\lambda_3 N^2|\psi_g|^2\right\}[\psi_g^*]^2 u_\nu = 0\end{aligned} \tag{21}$$

where

$$\mathcal{L}_\nu \equiv H_0 - \mu + 2U_0 N\left|\psi_g\right|^2 + 3\lambda_3 N^2|\psi_g|^4. \tag{22}$$

H_0 is the harmonic oscillator Hamiltonian, $U_0 \equiv -(4\pi\hbar^2|a|)/m$, ω_ν is the frequency of the collective oscillations, N is the number of atoms and $\psi_g \equiv \psi_g(\boldsymbol{r})$ is the ground state solution of equation (7). The above equations have been solved by using several methods [38, 39, 41]. In the present calculations we have employed two methods: a time-dependent and a time-independent one. In the time-dependent procedure we have added a weak perturbation to the potential and, with the CN algorithm, examined the time evolution of equation (6) for a selected point of the wavefunction. The lowest collective oscillations (ω_ν) were determined

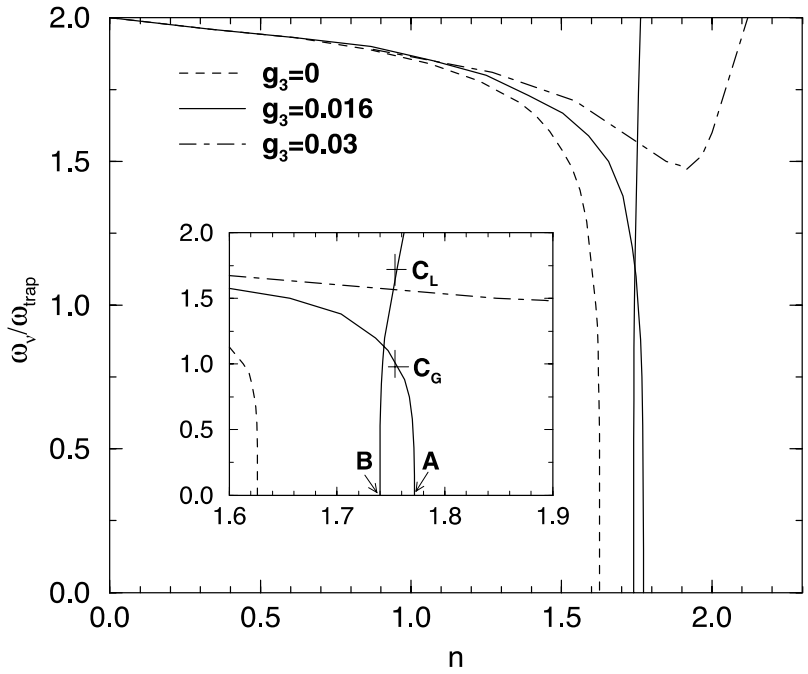

Figure 6. Collective frequencies as a function of the reduced number of atoms n. The inset shows the critical points corresponding to the previous figures.

through Fourier transformation [39]. By using the time-independent algorithm, we have solved equations (21) with the matching algorithm [42] generalized for two functions u and v. The method works by departing from the analytically known u, v and ω_ν for the harmonic oscillator (the chemical potential near to $3/2\hbar\omega$). Then we successively apply the matching method for the coupled u and v, gradually decreasing the chemical potential. This allows one to reach subsequent solutions, by employing the deformation algorithm described in [35]. We obtain exact agreement between both methods, time-dependent or time-independent.

Figure 6 shows the collective frequencies ω_ν as a function of n for the first mode ($l = 0$). The solutions corresponding to $g_3 = 0$ agree well with those given in [38], losing stability as $\omega_\nu \to 0$. By using this criterion, we have obtained the regions of stability for $g_3 = 0.016$. For $g_3 = 0.03$ all the solutions are stable. Following the inset of figure 6, for $g_3 = 0.016$, one can observe that, as the number of atoms is increased, in the less dense phase, the frequency of the collective excitations decreases and is related to stable solutions up to the point C_G; from this point down to the point A (increasing n), the frequency continues to decrease to zero, but now related to metastable solutions. As already explained previously in the discussion of figures 2–5, and also from the variational energy solutions given in figure 1, it is very likely that a phase transition occurs, from C_G to C_L (or from the metastable solutions, given in the branches C_G–A and B–C_L, to the corresponding stable solutions with fixed n). Once in the denser phase (from B passing through the point C_L), the frequency of the collective excitations increases as the number of atoms increases, in contrast to the behaviour observed for the system in the less dense phase. This can be qualitatively understood considering the variational energy of the two phases and the corresponding stable energy as shown in figure 1. The curvature of the variational energy as a function of α at the minimum for the liquid phase is greater than the corresponding one in the gas phase (compare in figure 1 insets (I) and (II) with insets (III) and

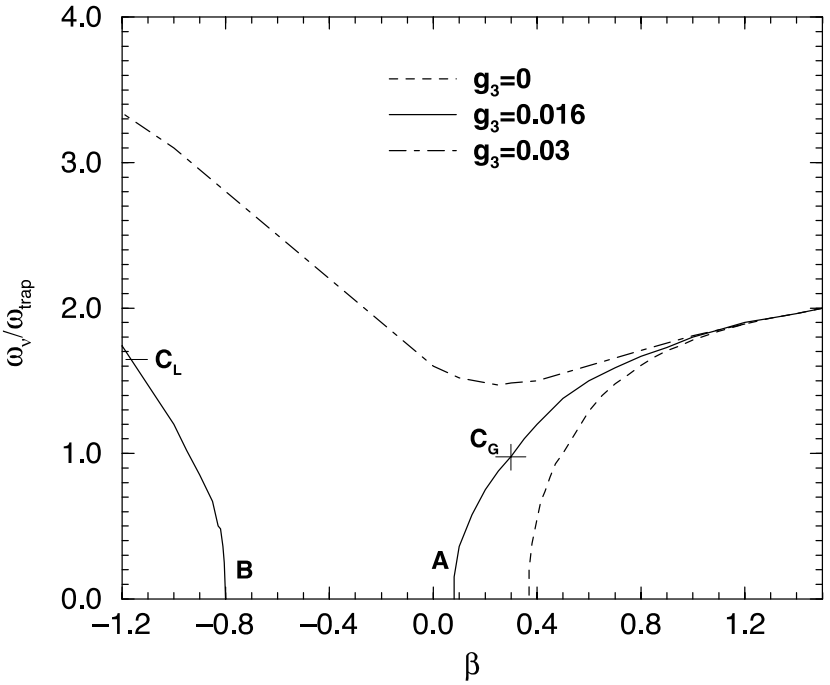

Figure 7. Collective frequencies as a function of the chemical potential β.

(IV)). This indicates, in agreement with figure 6, that the restoration force is stronger for the liquid phase than for the gas phase and consequently the frequencies of the collective modes starting at the point C_L are higher than the corresponding ones for the gas phase ending at C_G. As we include more particles the frequencies of the oscillations increase in the liquid phase. Corresponding to figure 6, in figure 7 the collective frequencies are shown as a function of the chemical potential β. From right to left, as the chemical potential decreases up to C_G, β also decreases; from C_G to A, and from B to C_L the solutions are metastable, such that the system will look for a transition to a stable branch (from C_G, increasing β, and from C_L, decreasing β). From C_L, as we further decrease the value of β the frequency of the collective excitations increases.

5. Conclusions

To summarize, we have presented results for the total energy, chemical potential and central density in terms of the number of atoms in the condensed state, for a range of values of the three-body strength. We also study the lowest collective mode excitations of the ground state.

Our calculation presents, at the mean-field level, the consequences of a repulsive three-body effective interaction for the Bose-condensed wavefunction, together with an attractive two-body interaction. A first-order liquid–gas phase transition is observed for the condensed state as soon as a small repulsive effective three-body force is introduced. In dimensionless units the critical point is obtained when $g_3 \approx 0.0183$ and $n \approx 1.8$. The characterization of the two phases through their energies, chemical potentials, central densities and collective excitations were also given for some values of the three-body parameter g_3. The results presented in this paper can be relevant to determine a possible clear signature of the presence

of repulsive three-body interactions in Bose-condensed atoms. It points to a new type of phase transition between two Bose fluids. Because of the condensation of the atoms in a single wavefunction this transition may present very peculiar fluctuations and correlation properties. Consequently, it may fall into a different universality class than the standard liquid–gas phase transition, which is strongly affected by many-body correlations. This matter certainly deserves further study.

Acknowledgments

This work was partially supported by Fundação de Amparo à Pesquisa do Estado de São Paulo and Conselho Nacional de Desenvolvimento Científico e Tecnológico.

References

[1] Bose S N 1924 *Z. Phys.* **26** 178
Einstein A 1924 *Sitz. Preuss Akad. Wiss.* **1924** 261
Einstein A 1925 *Sitz. Preuss Akad. Wiss.* **1925** 3
[2] Parkins A S and Walls D F 1998 *Phys. Rep.* **303** 1
Griffin A, Snoke D W and Stringari S 1995 *Bose–Einstein Condensation* (Cambridge: Cambridge University Press)
[3] London F 1938 *Phys. Rev.* **54** 947
London F 1954 *Superfluids II* (New York: Wiley)
[4] Bogoliubov N N 1947 *J. Phys. (USSR)* **11** 23
[5] Anderson M H, Ensher J R, Matthews M R, Wieman C E and Cornell E A 1995 *Science* **269** 198
[6] Bradley C C, Sackett C A, Tollet J J and Hulet R G 1995 *Phys. Rev. Lett.* **75** 1687
Bradley C C, Sackett C A and Hulet R G 1997 *Phys. Rev. Lett.* **78** 985
Bradley C C, Sackett C A, Tollet J J and Hulet R G 1997 *Phys. Rev. Lett.* **79** 1170
[7] Davis K B, Mewes M-O, Andrews M R, van Druten N J, Durfee D S, Kurn D M and Ketterle W 1995 *Phys. Rev. Lett.* **75** 3969
Andrews M R, Mewes M-O, van Druten N J, Durfee D S, Kurn D M and Ketterle W 1996 *Science* **273** 84
Mewes M-O, Andrews M R, van Druten N J, Kurn D M, Durfee D S and Ketterle W 1996 *Phys. Rev. Lett.* **77** 416
[8] Fried D G, Killian T C, Willmann L, Landhuis D, Moss A C, Greytak T J and Kleppner D 1998 *Phys. Rev. Lett.* **81** 3811
[9] Cornell E 1996 *J. Res. Natl Inst. Stand. Technol.* **101** 419
[10] Huang K 1987 *Statistical Mechanics* 2nd edn (New York: Wiley)
[11] Edwards M and Burnett K 1995 *Phys. Rev.* A **51** 1382
Ruprecht P A, Holland M J, Burnett K and Edwards M 1995 *Phys. Rev.* A **51** 4704
[12] Baym G and Pethick C J 1996 *Phys. Rev. Lett.* **76** 6
[13] Weiner J, Bagnato V S, Zilio S and Julienne P S 1999 *Rev. Mod. Phys.* **71** 1
[14] Kagan Yu, Muryshev A E, Shlyapnikov G V and Walraven J T M 1996 *Phys. Rev. Lett.* **76** 2670
[15] Akhmediev N, Das M P and Vagov A V 1997 *Condensed Matter Theories* vol 12, ed J W Clark and P V Panat (New York: Nova) pp 17–25
Akhmediev N, Das M P and Vagov A V 1999 *Int. J. Mod. Phys.* B **13** 625
[16] Gammal A, Frederico T and Tomio L 1999 Trapped Bose–Einstein condensed gas with two and three-atom interactions *Proc. Int. Workshop on Collective Excitations in Fermi and Bose Systems* ed C Bertulani, L F Canto and M Hussein (Singapore: World Scientific)
[17] Esry B D, Greene C H, Zhou Y and Lin C D 1996 *J. Phys. B: At. Mol. Opt. Phys.* **29** L51
[18] Josserand C and Rica S 1997 *Phys. Rev. Lett.* **78** 1215
[19] Kagan Yu, Svistunov B V and Shlyapnikov G V 1985 *JETP Lett.* **42** 209
[20] Fedichev P O, Reynolds M W and Shlyapnikov G V 1996 *Phys. Rev. Lett.* **77** 2921
[21] Burt E A, Ghrist R W, Myatt C J, Holland M J, Cornell E A and Wieman C E 1997 *Phys. Rev. Lett.* **79** 337
[22] Efimov V 1970 *Phys. Lett.* B **33** 563
Efimov V 1990 *Commun. Nucl. Part. Phys.* **19** 271
[23] Frederico T, Tomio L, Delfino A and Amorim A E A 1999 *Phys. Rev.* A **60** R9

[24] Ginzburg V L and Pitaevskii L P 1958 *Zh. Eksp. Teor. Fiz.* **34** 1240 (Engl. transl. *Sov. Phys.–JETP* **7** 858)
Gross E P 1963 *J. Math. Phys.* **4** 195
[25] Pitaevskii L P 1961 *Zh. Eksp. Teor. Fiz.* **40** 646 (Engl. transl. *Sov. Phys.–JETP* **13** 451)
[26] Gammal A, Frederico T, Tomio L and Chomaz Ph 2000 Liquid–gas phase transition in Bose–Einstein condensates with time evolution *Phys. Rev.* A **61** 051602(R)
[27] Gammal A, Frederico T, Tomio L and Abdullaev Kh F 2000 *Phys. Lett.* A **267** 305
[28] Kagan Yu, Muryshev A E and Shlyapnikov G V 1998 *Phys. Rev. Lett.* **81** 933
[29] Amorim A E A, Frederico T and Tomio L 1997 *Phys. Rev.* C **56** R2378
[30] Inouye S, Andrews M R, Stenger J, Miesner H J, Stamper-Kurn D M and Ketterle W 1998 *Nature* **392** 151
[31] Vuletic V, Chin C, Kerman A J and Chu S 1999 *Phys. Rev. Lett.* **83** 943
[32] Houbiers M and Stoof H T C 1996 *Phys. Rev.* A **54** 5055
[33] Fetter A L and Walecka J D 1971 *Quantum Theory of Many-Particle Systems* (New York: McGraw-Hill)
[34] Fetter A L 1996 *Phys. Rev.* A **53** 4245
[35] Gammal A, Frederico T and Tomio L 1999 *Phys. Rev.* E **60** 2421
[36] Ames W F 1992 *Numerical Methods for Partial Differential Equations* 3rd edn (New York: Academic) pp 111–5
[37] Stringari S 1996 *Phys. Rev. Lett.* **77** 2360
[38] Singh K G and Rokhsar D S 1996 *Phys. Rev. Lett.* **77** 1667
[39] Ruprecht P A, Edwards M, Burnett K and Clark C W 1996 *Phys. Rev.* A **54** 4178
Edwards M, Ruprecht P A, Burnett K, Dodd R J and Clark C W 1996 *Phys. Rev. Lett.* **77** 1671
[40] Fetter A L 1972 *Ann. Phys., NY* **70** 67
Fetter A L and Rokhsar D 1998 *Phys. Rev.* A **57** 1191
[41] You L, Hoston W and Lewenstein M 1997 *Phys. Rev.* A **55** R1581
[42] Giordano N J 1997 *Computational Physics* (Englewood Cliffs, NJ: Prentice-Hall) pp 257–72